WARWICK
THE UNIVERSITY OF WARWICK

Original citation:
Roukala, Juho, Orr, Simon T., Hanna, John V., Vaara, Juha, Ivanov, Alexander V., Antzutkin, Oleg N. and Lantto, Perttu. (2016) Experimental and first-principles NMR analysis of Pt(II) complexes with O,O´-Dialkyldithiophosphate ligands. The Journal of Physical Chemistry A, 120 (42). pp. 8326-8338.
Permanent WRAP URL:
http://wrap.warwick.ac.uk/84124

Copyright and reuse:
The Warwick Research Archive Portal (WRAP) makes this work by researchers of the University of Warwick available open access under the following conditions. Copyright © and all moral rights to the version of the paper presented here belong to the individual author(s) and/or other copyright owners. To the extent reasonable and practicable the material made available in WRAP has been checked for eligibility before being made available.

Copies of full items can be used for personal research or study, educational, or not-for profit purposes without prior permission or charge. Provided that the authors, title and full bibliographic details are credited, a hyperlink and/or URL is given for the original metadata page and the content is not changed in any way.

Publisher's statement:
"This document is the Accepted Manuscript version of a Published Work that appeared in final form in. The Journal of Physical Chemistry A. copyright © American Chemical Society after peer review and technical editing by the publisher.
To access the final edited and published work
http://pubs.acs.org/page/policy/articlesonrequest/index.html ."

A note on versions:
The version presented here may differ from the published version or, version of record, if you wish to cite this item you are advised to consult the publisher's version. Please see the 'permanent WRAP URL above for details on accessing the published version and note that access may require a subscription.

For more information, please contact the WRAP Team at: wrap@warwick.ac.uk

warwick.ac.uk/lib-publications

Experimental and first-principles NMR analysis of Pt(II) complexes with O,O'-dialkyl dithiophosphate ligands

Juho Roukala,*,† Simon Orr,‡ John V. Hanna,‡ Juha Vaara,† Alexander V. Ivanov,¶ Oleg N. Antzutkin,§,‡ and Perttu Lantto*,†

†*NMR Research Unit, University of Oulu, Oulu*

‡*Department of Physics, Warwick University, United Kingdom*

¶*Institute of Geology and Nature Management, Far Eastern Branch of the Russian Academy of Sciences, Russia*

§*Chemistry of Interfaces, Luleå University of Technology, Sweden*

E-mail: juho.roukala@oulu.fi; perttu.lantto@oulu.fi

Phone: +358 (0)294 48 1312

Abstract

Polycrystalline bis(dialkyldithiophosphato)Pt(II) complexes of the form $Pt\{S_2P(OR)_2\}_2$ (R = ethyl, *iso*-propyl, *iso*-butyl, *sec*-butyl or *cyclo*-hexyl group) were studied using solid-state ^{31}P and ^{195}Pt NMR spectroscopy to determine the influence of the alkyl substituents to the structure of the central chromophore. Measured anisotropic chemical shift (CS) parameters for ^{31}P and ^{195}Pt tensors affords more detailed chemical and structural information as compared to isotropic NMR parameters, such as chemical shifts and J-couplings, alone. The demanding theoretical modeling at hybrid DFT level including both crystal lattice and relativistic spin–orbit effects qualitatively reproduced

the experimentally observed CS tensors, thus supporting experimental analysis, as well as providing extensive orientational information for the tensors in the molecular frames. The results for ^{195}Pt CS tensors demonstrated that differences in alkyl substitutes of dialkyldithiophosphate ligands in the complexes studied have an insignificant effect on the distorted-square form structure of the central PtS_4 core. However, the principal values of ^{31}P chemical shift tensors in dialkyldithiophosphate ligands do differ significantly, which may be used to distinguish between different complexes. Relativistic effects (both scalar and spin–orbit) were shown to be important for the NMR parameters of both ^{31}P and ^{195}Pt nuclei. The effects due to the periodic crystal lattice were found to be non-negligible, especially for the CS tensor of the heavy-metal ^{195}Pt isotope. A particular correction model for incorporating lattice effects was adopted to avoid a severe deterioration of the anisotropic parameters due to the high requirements posed on the pseudopotential quality in such calculations. It seems that the pseudopotentials available in standard software may be inadequate for periodic calculations of anisotropic NMR parameters.

Introduction

Both experimental nuclear magnetic resonance (NMR) measurements and calculations of the chemical shift (CS) tensor parameters of heavy nuclei, such as ^{195}Pt, ^{207}Pb, etc., still constitute a challenge. The large chemical shift anisotropy (CSA), which can amount to a few thousand ppm, causes very wide spectral features in solid-state NMR. On the other hand, relativistic effects on the electronic structure have to be taken into account in the quantum-mechanical calculations of the NMR parameters.

Square-planar platinum(II) complexes featuring an intraorbital dsp^2 hybrid state of the central platinum atom are of interest mainly in medical applications. The high antitumor activity of *cis*−$[Pt(NH_3)_2Cl_2]$ (cisplatin, first generation) was first discovered by Rosenberg[1,2] in 1969. Since then, practical and important properties have also been established in other planar Pt(II) compounds, e.g., *cis*−$[Pt(NH_3)_2\{(OOC)_2C(CH_2)_3\}]$ (carboplatin, second generation),[3] and $[Pt\{1,2-(NH_2)_2(C_6H_{10})\}(OOC-COO)]$, (oxaliplatin, third generation).[4,5] Most of the presently known bis(dialkyldithiophosphato)platinum(II) complexes are liquid substances.[6] Therefore, only few crystalline platinum(II) *O*,*O*′-dialkyldithiophosphates have previously been studied.[6–12] A schematic representation of the complexes studied here is shown in Figure 1. The CSA of both ^{195}Pt and ^{31}P nuclei can be useful for studying the structures of these compounds, particularly in the case of Pt(II)-dialkyldithiophosphate

surface complexes, when other structural methods such as X-ray diffraction are not applicable because of the amorphous nature of samples.

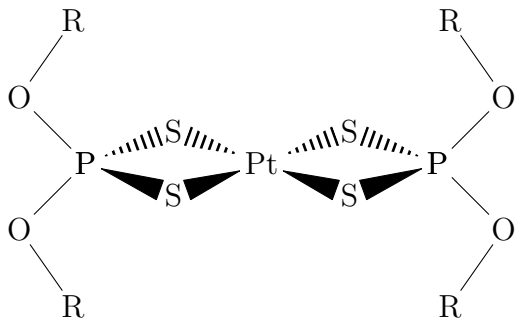

Figure 1: Schematic representation of the molecular structure of the Pt(II) *O*,*O*′-dialkyl dithiophosphates. The alkyl group R is one of C_2H_5 (compound I), *iso*-C_3H_7 (II), *iso*-C_4H_9 (III), *sec*-C_4H_9 (IV), or *cyclo*-C_6H_{11} (V).

A full analysis of the ^{195}Pt and ^{31}P CS tensors of five compounds of the form $Pt\{S_2P(OR)_2\}_2$ is reported in this study. For platinum(II) complexes with R=*iso*-C_4H_9,[9,11] R=*iso*-C_3H_7 and R=*cyclo*-C_6H_{11},[10] some of the experimental ^{195}Pt magic-angle-spinning (MAS) NMR data has been reported, while for compounds with R=C_2H_5 and R=*sec*-C_4H_9, the data are missing until now. Previous reports have revealed a clear difference between the ^{195}Pt CSA of cooperite (PtS)[13,14] and platinum(II) dialkyldithioposphates.[9–11] The former compound has a structure based on square planar [PtS_4] chromophores while the latter complexes form distorted squares, yet they maintain an almost axially symmetric ^{195}Pt CSA. Without a complete analysis of the platinum-195 CSA it has been, so far, impossible to determine whether the type of alkyl ligands has a significant effect on the degree of deviation from the square planar geometry.

As the ^{195}Pt CSA is too large for NMR data acquisition with a single frequency window, a summed Fourier-transform field-sweep technique[15] was employed in this work. This allowed for a fully automated acquisition of the entire lineshape without the need for normalizing intensities with respect to the frequency of acquisition, as would be required with a traditional frequency-stepping approach.[16] To complement experiments, a computational study was also performed in this work, yielding the ^{195}Pt and ^{31}P nuclear shielding tensors, as well as the Pt–P spin–spin *J*-coupling constants. Recently, Fu and Vaara calculated the relativistic ^{195}Pt and ^{31}P shielding tensors of the in vacuo bis(diethyldithiophosphato)platinum(II) complex.[17] To our knowledge, the present paper constitutes the first successful attempt at calculating the solid-state NMR properties in this family of Pt(II) complexes. Relativistic effects, arising due to the heavy metal, are here found to significantly affect the NMR properties of both ^{31}P and ^{195}Pt nuclei. A recent benchmark study[18] has also shown the importance of relativistic effects to the ^{31}P chemical shifts. The largest effect of the crystal lattice is to modify the isotropic chemical shifts of both ^{195}Pt and ^{31}P. The contribution to the CSA and asymmetry parameters of these two types of nuclei is smaller, but still noticeable, and should not be neglected if at least qualitative agreement with experiments is sought after. In this work a good agreement is obtained between theoretical and with experimental results, especially for phosphorus. Additionally, the sign of the spin–spin coupling constants and the directions of

the principal axes of the CS tensors are revealed from calculations. These are of a crucial importance for understanding the correlation between the structure and NMR spectra of the named platinum(II)-dialkyldithiophosphate complexes.

Experimental

Five crystalline complexes were obtained by reacting $K_2[PtCl_4]$ and salts of the form $K\{S_2P(OR)_2\}$ in aqueous solutions at 60°C overnight. The reaction products were filtered leaving yellow precipitates that were washed and left to dry. The following platinum(II)-dialkyldithiophosphate complexes were prepared using this protocol and abbreviated as: Pt-dtp-ethyl [bis(diethyldithiophosphato)platinum(II), compound I], Pt-dtp-*iso*-propyl [bis(di-*iso*-propyldithiophosphato)platinum(II), compound II], Pt-dtp-*iso*-butyl [bis(di-*iso*-butyldithiophosphato)platinum(II), compound III], Pt-dtp-*sec*-butyl [bis(di-*sec*-butyldithiophosphato)platinum(II), compound IV] and Pt-dtp-*cyclo*-hexyl [bis(di-*cyclo*-hexyldithiophosphato)platinum(II), compound V]. The X-ray diffraction structures [see Tables S1–S7 in the Supporting Information (SI)] of compounds III and IV contained two alternative conformations each, which are denoted with A and B, for both complexes.

All ^{195}Pt Static Field Sweep NMR data were obtained at 7.05 T using Chemagnetics CMX-300 spectrometer and a modified Magnex magnet equipped with a secondary superconducting coil capable of sweeping the field ±0.5 T. The current to the secondary coil was controlled by the spectrometer through a Lakeshaw magnet power supply. All measurements were undertaken using a Bruker Z33V HP static probe, with approximately 200 mg of each sample packed into 9.5 mm PTFE sample holders, which were accommodated in the horizontal solenoid arrangement of this probe. In order to isolate the very rapidly decaying free induction decay (FID) signal from probe ringing, a $\pi/2$–τ–π–τ Hahn echo sequence was used. The lengths of the $\pi/2$ and π pulses were 5 μs and 10 μs, respectively, and τ delay was 15 μs. A recycle delay of 4 s was implemented for complex II, while complexes I, III A, III B, IV A, IV B and V required a longer recycle delay of 35 s. All ^{195}Pt isotropic chemical shifts, δ_{iso}, were referenced to the sharp single resonance line of 1M $K_2Pt(CN)_6$ (aq.) at $\delta_{iso} = -3866$ ppm (external reference). The field sweeps were initiated with zero current in the secondary coil and a resultant field of 7.05 T, with the probe being tuned to 64.08 MHz, which is below the known low-frequency edge of each measured ^{195}Pt lineshape. For complexes II–V the current was then increased to 1.2963 A in six equal increments of 216 mA, each of which reduced the resultant field applied at the sample. For complex II 11000 transients were acquired at each field value, while for complexes III A–V 5100 transients were acquired. For complex I the current was increased to 1.080 A in five equal increments of 216 mA with 7400 transients acquired at each field value. The current in the secondary coil is linked to the frequencies F of the spins at 7.05 T by $A_{max} = B_0C(F_{max} - F_{min})/F_{min}$. In this case F_{max} and F_{min} are 64.38 and 64.08 MHz, respectively, and $C = 0.0254615$ is a constant that depends on the particular properties of the secondary coil.[19]

The data at each field value was Fourier transformed and processed with 5 kHz of exponential line broadening prior to shifting the frequency axis by $\Delta F = -(F_{max} - F_{min})/(N_{slices} - 1) =$ 50 kHz with respect to the previous spectrum. This shifted each spectrum to the corresponding frequency at $B_0 = 7.05$ T. The spectra were then summed to reconstruct the total

lineshape. As this technique relies on the recreation of a lineshape with a greater span than the equipment is capable of exciting at a single field value, the gap between each spectrum must be considered carefully. If the spectra are widely enough separated, the lineshape will become distorted by the excitation profiles of the individual spectra. Modeling the response of both the spins and the spectrometer show that this effect becomes visually insignificant when ΔF is less than or equal to $1.5\delta F$, where $2\delta F$ is the full width at half maximum of an individual spectrum.[19] It is observed that the FWHM width of an excitation and response was ca. 75 kHz for a $\pi/2$ pulse length of 5 μs, so the condition $\Delta F < 56$ kHz is fulfilled. Each summed ^{195}Pt broadline spectrum was simulated using a static CSA lineshape function using the Dmfit software package.[20]

All ^{31}P CPMAS NMR data were recorded at 7.05 T using a Chemagnetics CMX-300 console operating at a ^{31}P Larmor frequency of 121.482 MHz. The ^{1}H–^{31}P cross-polarization experiment was used in conjunction with continuous wave proton decoupling at 300.098 MHz to suppress heteronuclear dipolar interactions. These measurements were undertaken using a Bruker 4 mm HX probe which enabled MAS frequencies of 2–4 kHz. The ^{1}H $\pi/2$ pulse length was 3.5 μs, the contact time 2 ms, and the recycle delay 3 s. The ^{31}P chemical shifts were indirectly referenced to 85% H_3PO_4 ($\delta_{iso} = 0.0$ ppm) via a secondary solid $NH_4H_2PO_4$ reference at $\delta_{iso} = 0.9$ ppm.[21] The ^{31}P chemical shift anisotropy parameter, δ_{aniso}, and the asymmetry parameter, η, of the chemical shift tensor were calculated using the Mathematica program of Levitt and co-workers,[22] based on an analysis of χ^2 statistics. Plotting of the diagrams was based on a quantitative analysis of the integrated intensity ratios of the spinning sidebands in the spectra, recorded at two different spinning frequencies. The calculations were performed using the Mathematica program (version 4.1.2).[23]

Computational

First-principles density functional theory (DFT) calculations of the NMR shielding tensors $\boldsymbol{\sigma}$ were performed using both solid-state and single-molecule methodologies with the CASTEP[24–27] and Amsterdam Density Functional[28–31] (ADF) codes, respectively, with the latter program also used in the computation of spin–spin J-couplings. Nonrelativistic calculations were performed with ADF (see SI for more details). The zeroth-order regular approximation[32] (ZORA) method was utilized both in CASTEP and ADF to treat relativistic effects, through scalar-relativistic (SR) pseudopotentials[33] in the former, and at the 1-component SR and 2-component spin–orbit (SO) levels in the latter one. The fully relativistic ReSpect[34] program based on 4-component theory was used to benchmark the ADF calculations (see Tables 30 and 31 in SI). A unit cell with $6 \times 5 \times 4$ k-points and a cutoff energy of 750 eV was used in CASTEP for crystal calculations, while $3 \times 3 \times 3$ k-points were used for periodic calculations at the molecular limit (a single molecule in a cubic cell with a side length of 20 Å). The molecular calculations employed all-electron jcpl/TZP basis sets[35] for Pt and P/other atoms in ADF, and Dyall's cvtz-level basis sets[36] for all atoms in ReSpect. The parameter-free PBE[37] density functional was used in all codes, with additional PBE0[38,39] hybrid functional calculations performed with ADF. Calculations were performed for both A and B conformations of complexes III and IV.

The reported computational results (vide infra) were obtained using geometry-optimized

structures, where both the ions and the cell parameters were relaxed using CASTEP at the "fine" level with ultrasoft pseudopotentials,[40] a cutoff energy of 340 eV, and k-point grids 3×3×2 (compound I), 4×3×2 (II), 3×3×3 (III), 4×3×2 (IV), and 2×3×2 (V). The unit cells of compounds I and V contained two molecules each, whereas compounds II–IV contained one molecule per unit cell. The effect of geometry optimization to the NMR parameters was studied at the SR solid-state level of theory (vide infra).

Crystal lattice effects were found to be non-negligible for the shielding tensors, necessitating solid-state calculations. A molecular model, on the other hand, allowed evaluating the relativistic effects due to the heavy platinum atom more thoroughly, especially the SO effect, as well as assessing the impact of using a hybrid DFT functional. Both features are known to affect the shielding tensors of heavy-element compounds.[41,42] Lacking software capable of performing solid-state NMR calculations at the SO-coupled relativistic level of theory, with a hybrid DFT functional, a combination of solid-state and molecular approaches was used here to arrive at the final results. This is in contrast to the other theoretical studies of ^{195}Pt shielding in solid-state complexes,[43,44] where the relativistic and ligand-field effects have not been considered simultaneously.

For each complex, the ligand-field effect was calculated in CASTEP as the difference between a solid-state crystal calculation with the PBE functional, and another one where a single molecule was isolated in a cubic cell with a side length of 20 Å. This was taken as a correction to the base result, the shielding tensor calculated at the SO ZORA relativistic level using a hybrid PBE0 functional, in ADF. The corrected total tensors were obtained by summing the corresponding individual shielding tensor components σ_{ij} as

$$\sigma_{ij}^{\text{corr.}} = \sigma_{ij}^{\text{SO PBE0, molecule}} + (\sigma_{ij}^{\text{SR PBE, solid}} - \sigma_{ij}^{\text{SR PBE, isolated molecule}}) \tag{1}$$

after which the resulting principal components of the shielding tensors were obtained by diagonalizing the symmetric part of the tensor. It should be noted that, with an increasing cell size, especially the ^{195}Pt CS parameters obtained from periodic calculations with an isolated molecule in a large unit cell converged to clearly different values as compared to those obtained from a molecular calculation at roughly the same level (SR PBE). This may indicate a problem with the pseudopotential used in CASTEP; see SI for more details.

The shielding tensors are analyzed in terms of the isotropic shielding constant σ_{iso}, chemical shift δ_{iso}, the CSA parameter δ_{aniso}, and the asymmetry parameter η,

$$\delta_{\text{iso}} = \frac{\sigma_{\text{iso}}^{\text{ref}} - \sigma_{\text{iso}}}{1 - \sigma_{\text{iso}}^{\text{ref}}} \approx \sigma_{\text{iso}}^{\text{ref}} - \sigma_{\text{iso}}, \quad \text{when } \sigma_{\text{iso}}^{\text{ref}} \text{ is small} \tag{2}$$

$$\delta_{\text{aniso}} = \delta_{zz} - \delta_{\text{iso}} \tag{3}$$

$$\eta = \frac{\delta_{yy} - \delta_{xx}}{\delta_{zz} - \delta_{\text{iso}}}, \tag{4}$$

where δ_{zz}, δ_{yy} and δ_{xx} are the principal components of the chemical shift, labeled in such a way that $|\delta_{zz} - \delta_{\text{iso}}| \geq |\delta_{xx} - \delta_{\text{iso}}| \geq |\delta_{yy} - \delta_{\text{iso}}|$. Also the spin–spin J-coupling constants $^2J(^{195}\text{Pt}–^{31}\text{P})$ were studied. Our results support the findings of a computational study of ^{31}P spin–spin J-couplings in dioxaphosphorinanes,[45] where DFT was shown to qualitatively reproduce the experimentally observed J-coupling constants (see SI for more details).

The calculations were performed at an optimized geometry that represents a minimum energy structure of the PBE functional. The choice of the geometry (vide infra) was based on SR CASTEP shielding tensor calculations at three different levels of optimization. First, only hydrogen positions were optimized (H-opt., see Tables 8–14 in SI) while keeping the unit cell parameters fixed to their experimental values; then all ions were optimized (I-opt., Tables 15–21 in SI), and finally also the unit cell was relaxed (A-opt., Tables 22–28 in SI).

Results

Solid-state NMR Data

The ^{31}P NMR signals of all the complexes under study, shown in Figure 2 (a), are clearly split into three resonance lines with relative intensities ca. 1:4:1. A 1:1 doublet (satellite resonance lines) is a result of ^{195}Pt–^{31}P spin–spin J-coupling with a coupling constant of ca. 430–450 Hz. The natural abundance of ^{195}Pt (33.83%) explains the relative intensities of the satellites. A single wide feature is observed in the spectrum of Pt{S_2P(O-*sec*-$C_4H_9)_2$}$_2$, where the shape and asymmetry of the spectrum suggest a J-coupled split signal broadened to a much greater extent than the spectra of the other complexes. It is proposed that this is caused by the presence of six chiral isomers of the Pt-dtp complex, as explained in Ref. 12

Inspection of the sideband intensities in the ^{31}P MAS NMR spectra [see Figure 2 (a)] of all the complexes suggests a nearly rhombic symmetry of the chemical shift tensor of all the complexes. Statistical estimates of the ^{31}P CSA parameters were made by plotting the χ^2 diagrams of δ_{aniso} and η from the spinning sideband analysis. The range of values $\eta = 0.57$–0.98 (see Table 1 below) obtained for the complexes suggests a configuration close to a perfectly rhombic arrangement ($\eta = 1$). The values of δ_{aniso} range from ca. -30 to -45 ppm for different Pt-dtp complexes in this study.

In contrast to the ^{31}P NMR data, the lineshapes of the static ^{195}Pt NMR spectra [see Figure 2 (b)] of all the complexes correspond to an almost axially symmetric CS tensor. They are of a form similar to the spectrum of polycrystalline cooperite[13,14] (natural PtS) and suggest that the platinum atom is held in a configuration close to the square chromophores (PtS_4) found in cooperite. However, the value of the δ_{zz} component of the ^{195}Pt CS tensor for these complexes is much smaller than that observed in PtS, leading also to a substantial difference in the isotropic shifts. Fitting of the CSA lineshapes in dmfit was possible with a good agreement for all the complexes. The systems were observed to have very similar values of δ_{aniso}, within 140 ppm of one another (see Table 2). The complex I has a smaller anisotropy and, correspondingly, a more negative isotropic shift, which perhaps indicates a closer crystal packing in the direction perpendicular to the PtS_4 chromophore, which would follow intuitively from the smaller ligand size. The complex IV has the largest experimental anisotropy parameter, which could correspond to a weaker shielding from looser molecular packing. This may be caused by disorder due to the chiral polymorphism of ligands, which is referred to earlier. The values of η for the ^{195}Pt CS tensor have also been estimated for the first time and show little variance among the systems, and no correlation with δ_{aniso}. This suggests that there is little variation in the extent of the tetrahedral distortion of the PtS_4 chromophore between the complexes.

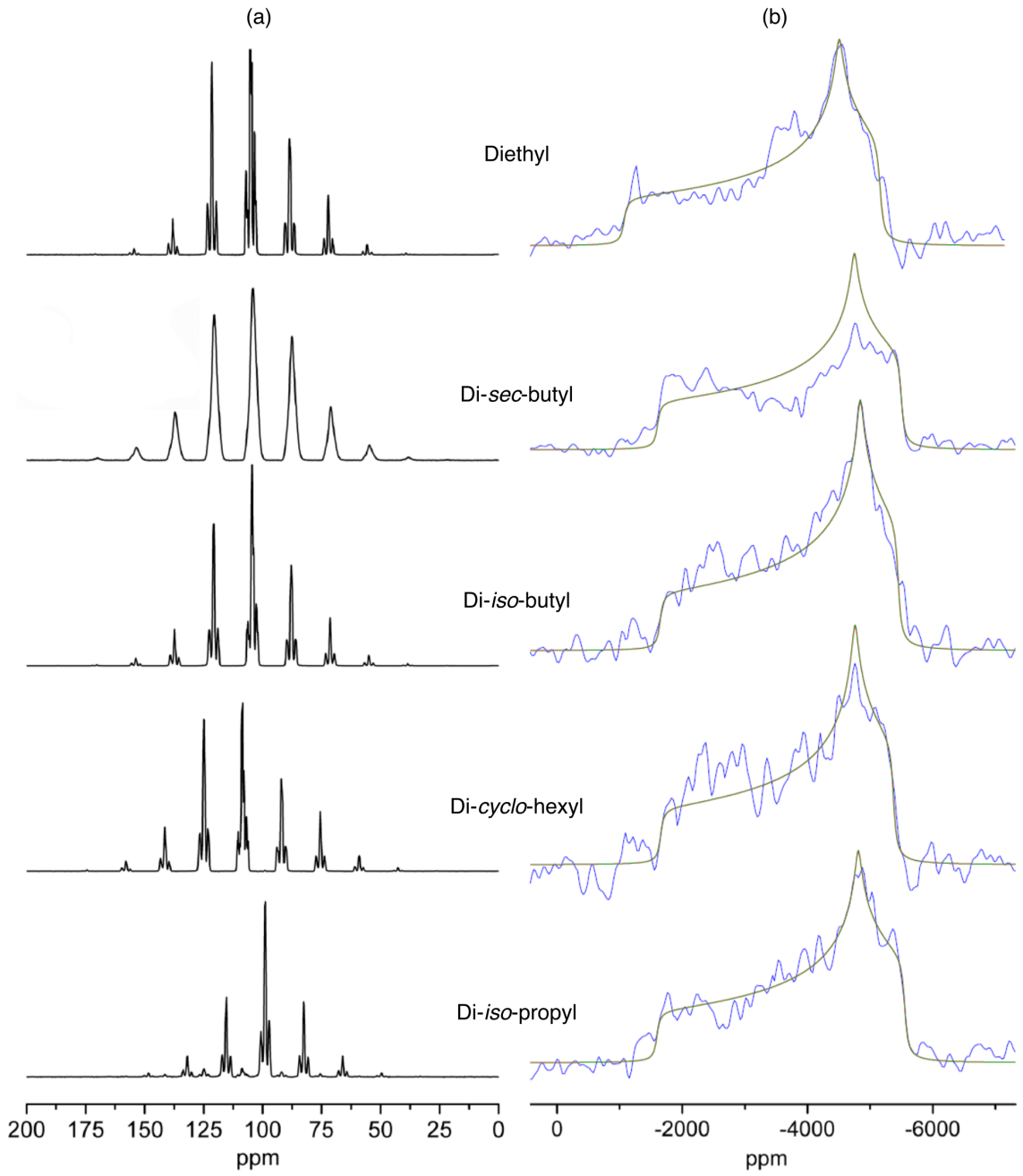

Figure 2: NMR spectra of $Pt\{S_2P(OR)_2\}_2$ complexes: (a) ^1H–^{31}P CP MAS NMR spectra, with a spinning frequency of 2 kHz. (b) Static ^{195}Pt field-sweep NMR spectra (blue lines) and static CSA models from Dmfit (black lines),[20] 5 kHz of broadening has been applied to both the spectra and the models.

Table 1: Calculated and experimental ^{31}P shielding tensor parameters in compounds I–V.

Compound[a]	Theor. σ_{iso}[b] (ppm)	Exp. δ_{iso}[c] (ppm)
I	236.8	105.0
II	239.4	108.5
III A	237.9	104.3
III B	237.6	
IV A	244.6	104.1
IV B	237.1	
V	244.1	99.0
Compound	Theor. δ_{iso}[d] (ppm)	Exp. δ_{iso}[d] (ppm)
I	2.6	−3.5
II	0.0	0.0
III A	1.6	−4.2
III B	1.9	
IV A	−5.2	−4.4
IV B	2.4	
V	−4.7	−9.5
Compound	Theor. δ_{aniso}[e] (ppm)	Exp. δ_{aniso} (ppm)
I	−31.3	−35.1±0.2
II	39.3	−42.7±0.2
III A	32.4	−38.1±0.1
III B	−36.4	
IV A	44.5	−43.3±0.2
IV B	41.2	
V	27.7	−30.8±0.2
Compound	Theor. η	Exp. η
I	0.56	0.57±0.03
II	0.91	0.75±0.02
III A	0.94	0.73±0.01
III B	0.63	
IV A	0.66	0.89±0.02
IV B	0.95	
V	0.68	0.98±0.02

[a]Pt-dtp-R, R: ethyl (I), *iso*-propyl (II), *iso*-butyl (III), *sec*-butyl (IV), and *cyclo*-hexyl (V). A and B refer to the two different conformations of the same complex.
[b]ADF SO-ZORA calculation with the PBE0 hybrid functional, added with ligand field correction from CASTEP and using optimized geometry (ions and cell parameters, CASTEP).
[c]Referenced to the peak of ammonium dihydrogen phosphate at 0.9 ppm.[21] See Refs. 12 (I, IV), 10 (II, V), and 9 (III).
[d]Referenced to compound II.
[e]Positive sign in some of the calculated ^{31}P CSAs results from a nearly symmetric NMR spectrum, where a small shift in δ_{yy} may swap the labels of δ_{xx} and δ_{zz}.

Table 2: Calculated and experimental ^{195}Pt shielding tensor parameters in compounds I–V.

Compound[a]	Theor. σ_{iso}[b] (ppm)	Exp. δ_{iso}[c] (ppm)
I	5855.6	−4030
II	5784.7	−4002.0
III A	5849.4	−4029.7
III B	5869.8	
IV A	5817.4	−3890
IV B	5788.0	
V	5793.9	−3963.6
Compound	**Theor. δ_{iso}[d] (ppm)**	**Exp. δ_{iso}[d] (ppm)**
I	0.0	0.0
II	70.9	28.0
III A	6.3	0.3
III B	−14.2	
IV A	38.2	140.0
IV B	67.6	
V	61.7	66.4
Compound	**Theor. δ_{aniso} (ppm)**	**Exp. δ_{aniso} (ppm)**
I	2318.3	2250.0
II	2322.7	2340.0
III A	2392.3	2340.0
III B	2276.6	
IV A	2311.2	2390.0
IV B	2258.2	
V	2231.9	2330.0
Compound	**Theor. η**	**Exp. η**
I	0.29	0.23
II	0.33	0.23
III A	0.33	0.26
III B	0.30	
IV A	0.36	0.25
IV B	0.36	
V	0.35	0.25

[a]Pt-dtp-R, R: ethyl (I), *iso*-propyl (II), *iso*-butyl (III), *sec*-butyl (IV), and *cyclo*-hexyl (V). A and B refer to the two different conformations of the same complex.
[b]ADF SO-ZORA calculation with the PBE0 hybrid functional, added with ligand field correction from CASTEP and using optimized geometry (ions and cell parameters, CASTEP).
[c]Referenced to the peak of $K_2Pt(CN)_6$ at −3866 ppm.
[d]Referenced to compound I.

Computational

The calculated isotropic shielding constants, chemical shifts, CSA parameters, and asymmetries in compounds I–V are shown in Tables 1 and 2 for ^{31}P and ^{195}Pt, respectively. The chemical shifts are reported relative to the complex with the largest absolute experimental chemical shift, this is compound II for ^{31}P and compound I the case of ^{195}Pt. Scalar relativistic effects were estimated using the molecular model and X-ray structures, and were found to be important in all complexes (see SI and Tables 30 and 31 therein for more details). The following discussion is based on results where the SR effects are accounted for.

Phosphorus-31

Figure 3 reveals that the calculations are found to yield good CSA and asymmetry parameters for ^{31}P in complexes I–V, as compared to experimental data, both in the solid-state and molecular models. The ligand-field corrected, SO-coupled relativistic level of calculation offers a slight improvement over the other approaches (where either SO-coupling and hybrid, or ligand field are missing), but due to the smallness of the various contributions, all the methods produce similar results. Isotropic ^{31}P shielding constants are in the range 237–245 ppm and gain positive contributions from SO coupling (ca. 19%), use of hybrid functional (ca. 4%) and the ligand field (less than 1.5%) in all compounds (see Table 32 in SI). Their impact to the experimental observable, the isotropic chemical shift, is much smaller because of the high similarity of the values among this group of molecules, leading to large cancellation. The experimental chemical shifts relative to compound II are small, ca. -4 ppm for compounds I, III, and IV, and almost -10 ppm for V. Their computational counterparts are in the same very narrow magnitude range, although no quantitative match is obtained within it.

The ^{31}P CSA parameter is found to be positive in most calculations, with compounds I and III B being the only ones having a negative CSA parameter at the ligand-field corrected SO ZORA level of calculation (see Table 1). This is due to the highly symmetric ^{31}P NMR spectrum, where $\delta_{yy} \approx \frac{1}{2}(\delta_{xx} + \delta_{zz})$. Thus, even a small change in δ_{yy} relative to the two other components may swap the labels xx and zz, resulting in a sign change in the parameter.

The asymmetry parameter is a delicate property to calculate, as demonstrated by the mutually partly cancelling contributions due to geometry, hybrid functional and SO effects, which are positive for ^{31}P η in some compounds and negative for some (vide infra). The ligand-field corrected computed asymmetry parameters are, however, larger than 0.5 in all complexes, with II, III A and IV B having $\eta \approx 0.9$ (see Table 1), meaning nearly rhombic CS tensors.

The computational results agree qualitatively with experiments in all the compounds, and the remaining differences are expected to be, at least partly, due to errors introduced by the chosen computational model. The different basis sets employed in the different programs (plane waves in CASTEP, Slater-type functions in ADF, and Gaussian functions in ReSpect), for example, are a source of error until the basis set limit, which is difficult to reach for systems of this size. The numerical accuracy is also dependent on the integration grids and convergence criteria, which may ultimately have an effect on the final results. Even if these errors are small within a single program, their cumulative effect may be more visible when the outcomes from several programs are combined into a single result.

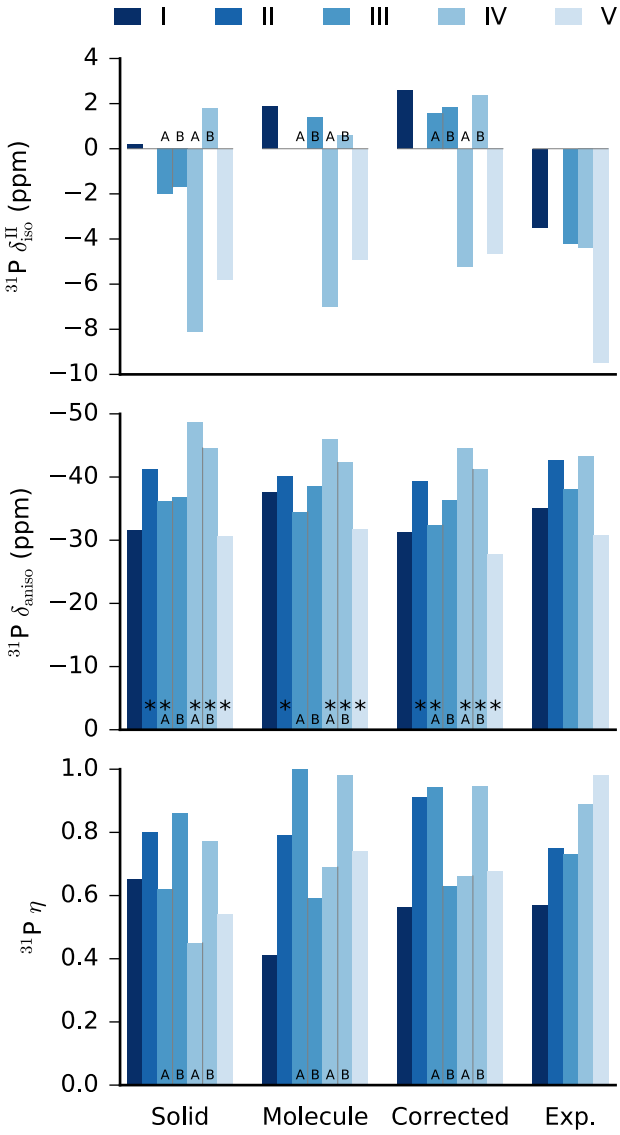

Figure 3: Comparison of the calculated and experimental values of ^{31}P chemical shift parameters, δ_{iso} (CS, top), δ_{aniso} (CSA parameter, middle), and η (asymmetry, bottom) in compounds I–V. The three leftmost groups of bars in each panel correspond to calculations at the SR level in solid state (PBE functional), SO ZORA level in a molecular model (PBE0 functional), and the molecular results corrected with the ligand-field contribution, correspondingly. Columns annotated with an asterisk * are actually positive, but negated here for easier comparison; see text for details. Bars annotated with A or B refer to two different conformations of the same complex in the crystallographic unit cell.

Geometry optimization. The changes to the CS, as well as the CSA and asymmetry parameters due to the optimization of the hydrogen atoms, then all ions, and finally also the unit cell parameters, is shown graphically in Figure 4, where the difference of the parameters with respect to the experimental values is plotted. The corresponding numerical data are presented in Tables 30, 31, 32, and 33 in SI. The most notable benefit, obtained at the point

where the geometry was optimized for all the ions, is to reduce the greatly overestimated ^{31}P CSA in compound IV to a level that agrees well with experiments. Optimization of only hydrogens introduces very small changes, which nevertheless demonstrate the sensitivity of NMR to structural modifications. Relaxing the unit cell parameters in addition to all ions only has a little effect to the phosphorus CSA, mainly canceling the difference between the A and B conformations of compound III, which was introduced by the cell-constrained ion optimization. The asymmetry parameter is relatively more affected, but in a less consistent way.

Solid-state and molecular models. The ^{31}P chemical shifts relative to compound II gain a relatively large positive contribution (up to ca. 2 ppm) from the ligand field, as seen in Figure 5 (the corresponding numerical data are presented in Tables 32 and 33 in SI), although the absolute changes are small due to small absolute values of the thus referenced CS values. The contributions to the CSA and asymmetry parameters are smaller in comparison to the two other contributions (exact exchange and SO-coupling), up to ca. 6 ppm and 0.16, respectively. As seen in Figure 5, the main effect of the ligand-field correction is to induce small relative changes between the CS parameters in different compounds.

Hybrid DFT functional. The partial inclusion of Hartree–Fock exchange into the DFT functional was studied at the SR level of theory in the molecular model. The use of the hybrid functional PBE0 (25% exact exchange) increases slightly the ^{31}P chemical shifts with respect to compound II in all complexes, as shown in Figure 5, except IV B where the contribution is zero. The magnitude of the CSA parameter is increased in all compounds except for IV A, where the inclusion of HF exchange yields a very small decrease. The asymmetry parameter is less consistently affected by the hybrid functional, with positive contributions in III A, IV A and V, and negative ones in the others.

Spin–orbit correction. While a relatively light element itself, phosphorus is also influenced by the so-called HALA (heavy-atom effects on the light atom[46,47]) relativistic effects due to the vicinity of the heavier atoms (S, Pt). The ^{31}P chemical shift, referenced to compound II, gains positive contributions from the SO-coupling at the ZORA level of theory in all complexes, as seen in Figure 5, although the change in compound V is negligibly small. In compounds I and III, the SO-contribution to CS is larger than the sum of the corresponding hybrid and ligand-field modifications. The phosphorus CSA and asymmetry parameters gains both positive and negative contributions of varying magnitude, depending on the complex. Except for the asymmetry parameter in compounds II and III A, the SO and hybrid functional contributions to the ^{31}P δ_{aniso} and η have opposite signs, with the magnitude of the SO-coupling being slightly smaller in most cases.

Based on the results, all the contributions are numerically significant, although there is some cancellation between them in the total parameters, as seen in Figure 5. Thus, the present approach of combining several calculations to include all the effects is justified, even if it does introduce a source of error as noted earlier.

Platinum-195

Unlike the CS tensor parameters of ^{31}P, those of ^{195}Pt require much more attention to obtain an agreement with experimental reference values for the right reasons. While the solid-state CASTEP calculation with X-ray ion positions and cell parameters appeared to produce

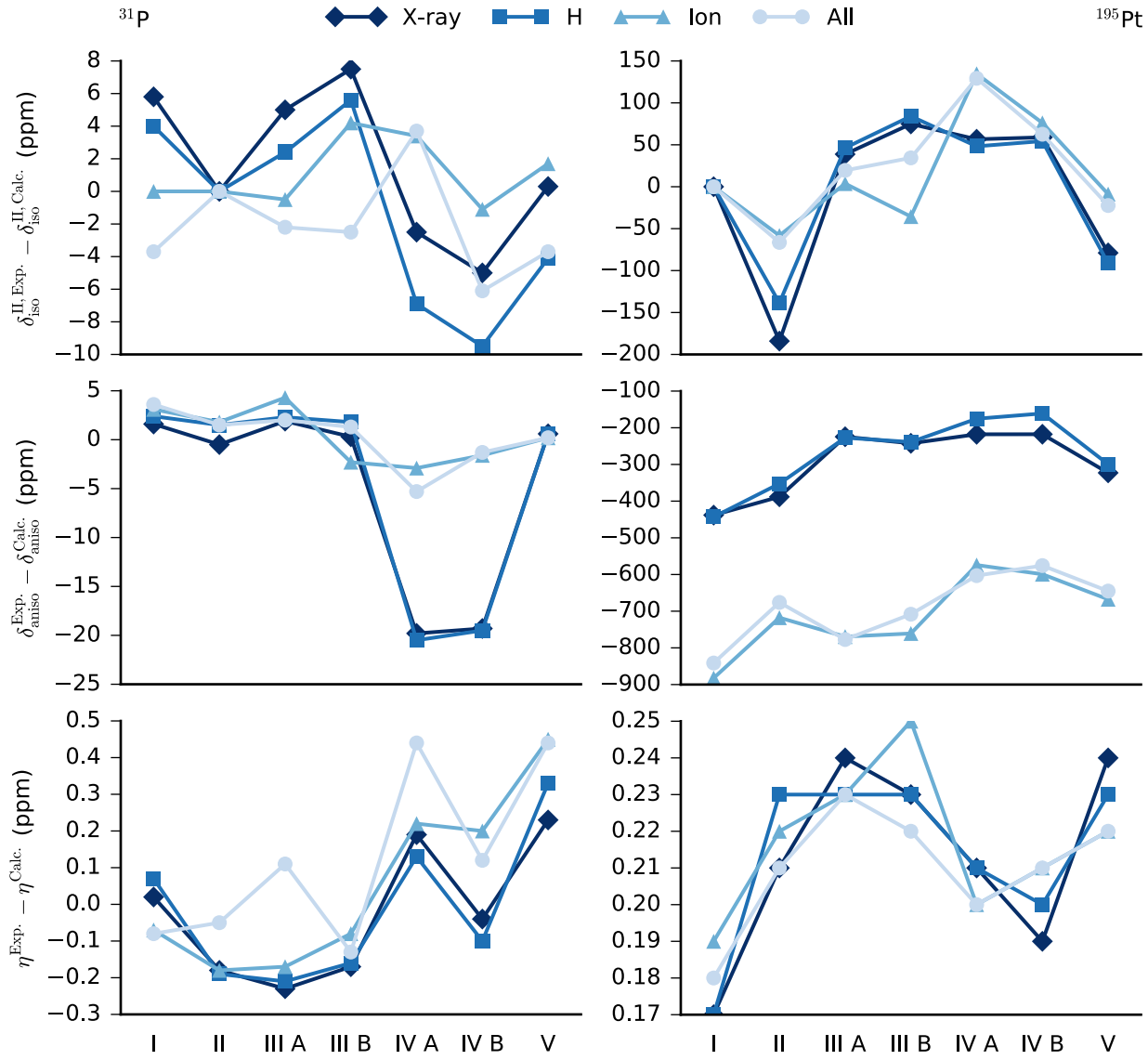

Figure 4: Effect of geometry optimization to the ^{31}P (panels on the left) and ^{195}Pt (right) chemical shift parameters. The plotted values show the difference in the parameters between the experimentally observed value (the zero line) and the fully, partially, or unoptimized (experimental X-ray) geometries. In the case of ^{31}P CSA parameters, the magnitudes $|\delta_{\text{aniso}}|$ are shown, to avoid comparison between positive and negative values (see text for more details). The large deviations of the ^{195}Pt CSA and asymmetry parameters from zero are due to the fact that CASTEP overestimates (underestimates) the calculated δ_{aniso} (η); see SI for details.

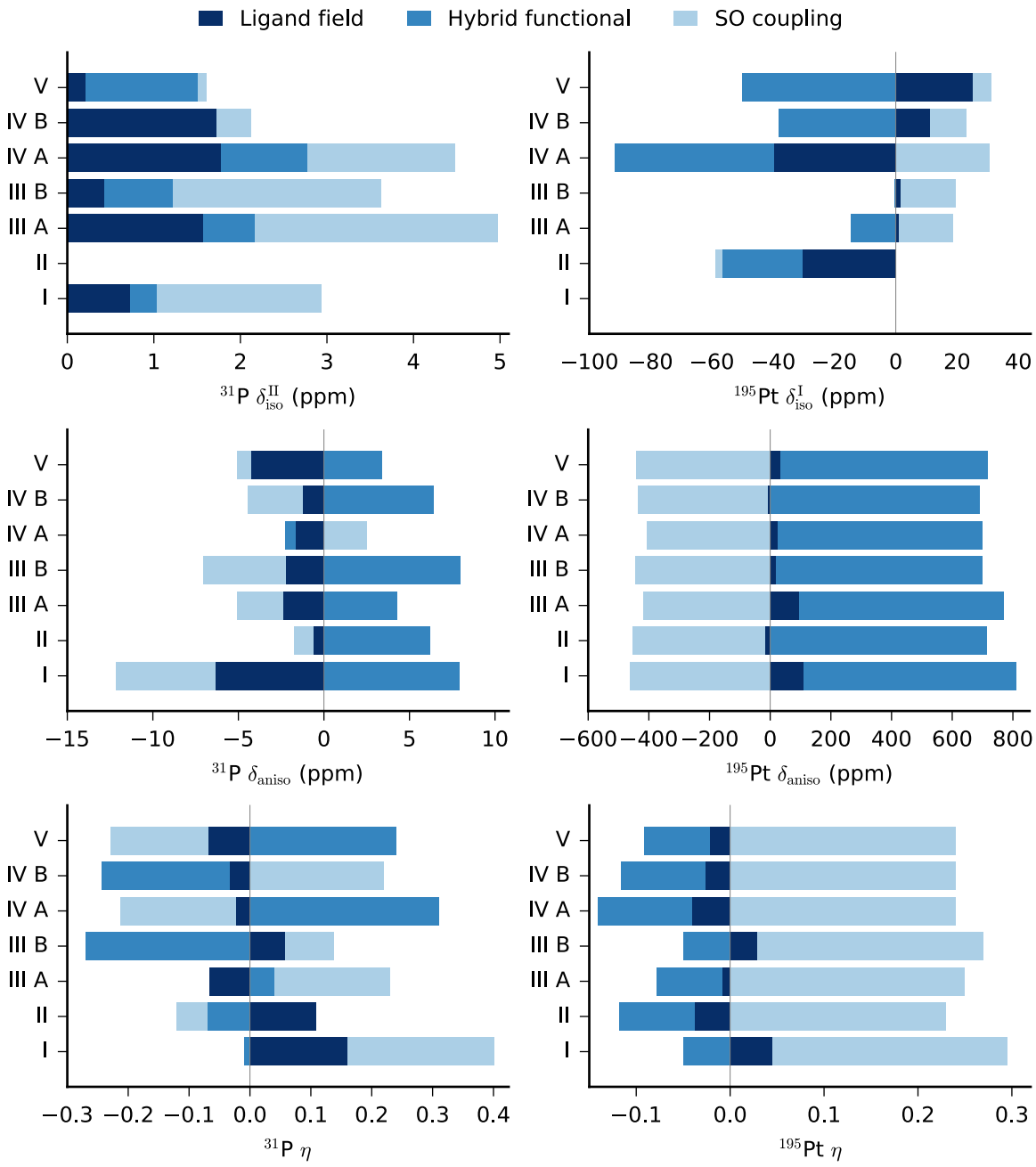

Figure 5: Contributions due to the ligand field, use of hybrid functional, and spin–orbit coupling to the ^{31}P (panels on the left) and ^{195}Pt (right) CS parameters, using the fully optimized geometries. The values denote the following differences: (solid-state)−(molecule-in-vacuum) calculation (Ligand field) at the periodic SR PBE level of theory, PBE0−PBE (Hybrid functional) at the molecular SR level of theory, and SO−SR calculation (SO coupling) at the molecular level, with PBE0. In the case of the ^{31}P CSA parameters, the magnitudes $|\delta_{aniso}|$ are shown, to avoid comparison between positive and negative values (see text for more details). The total values of each property are obtained by tensor component-wise summation as shown in (1), and not by summing these property differences, as explained in the text.

qualitatively correct relative chemical shifts for the studied compounds, as referenced to experimentally measured parameters, the approach failed to agree with the experimental CSA and asymmetry parameters. Notably, the periodic molecular-limit (CASTEP) calculations yielded much larger ^{195}Pt CS anisotropy and much smaller asymmetry parameters as compared to the SR molecular calculation (ADF), hinting at a problem with the pseudopotential used in CASTEP (see SI for more details). Thus, the solid-state calculation did not provide a good starting point for the theoretical modeling in this case. Instead, with an optimized geometry, the all-electron molecular calculation at the SO-coupled ZORA level of theory using the hybrid functional (PBE0) provided a better approximation, yielding already qualitative agreement with the experiments (see Figure 6), and adding the ligand-field effect further improved the lineshape corresponding to the ^{195}Pt CS tensor, as compared to experiments in Table 2. As with phosphorus, the isotropic ^{195}Pt shielding constants (5785–5870 ppm) and the contributions therein are nearly equivalent in all compounds, with spin–orbit coupling being the dominant one (ca. 55%) and ligand field the smallest (up to 1.7%). Unlike with phosphorus, the use of hybrid functional decreases the platinum shielding constants slightly in all compounds (by up to 7%, see Table 33 in SI). The following discussion is based on the experimentally observable isotropic CS, where cancellation again results in much smaller absolute contributions.

Considering the different complexes, little variation is found between them in the ^{195}Pt CSA and asymmetry parameters, as shown in Table 2. Especially the magnitude of the platinum CSA parameter is roughly equal (between 2200 and 2400 ppm) in all complexes. However, its value in compound I is consistently larger than in compound V (see Figure 6), irrespective of the geometry optimization and corrections due to SO-contribution and the use of hybrid functional. This is in contrast to experiments, even though the difference between the CSA parameters of compounds I and V is small both computationally and experimentally. The ^{195}Pt asymmetry parameters also show only small variations (up to 0.07 between the calculated values in I and IV) between the complexes, and while the calculated values are slightly larger (up to ca. 0.1) than their experimental counterparts, they agree that η is small, as compared to the same parameter for ^{31}P. These findings favor the idea that the central part of the complexes is more or less invariant to the different ligands, and therefore also the platinum shielding tensors are nearly equivalent in shape for Pt complexes with ligands belonging to the same class, i.e., dialkyl dithiophospates. A large anisotropy combined with a relatively small asymmetry translates to an axial, disc-shaped shielding tensor in the present case.

Geometry optimization. As with phosphorus, the relaxation of the hydrogen positions only introduces small changes, most visible in the ^{195}Pt CS of compound II (relative to compound I) and the CSA parameters in compounds II and IV, as shown in Figure 4. The largest change to the CS parameters is induced by the ion optimization, leading to a notable decrease of the CSs, and increase of the CSA parameters in all complexes. The asymmetry parameters are hardly affected by the optimization, remaining closer to zero than unity in all compounds. Relaxation of the cell parameters in addition to ions does not yield great changes, but does increase the magnitude of the ^{195}Pt CS in compound III relative to compound I. It should be noted that in Figure 4 the geometry optimization causes the CSA parameters to move further away from zero, i.e., the experimental reference values, because the CASTEP calculations overestimate the parameter, which was attributed to the pseudopotential (see

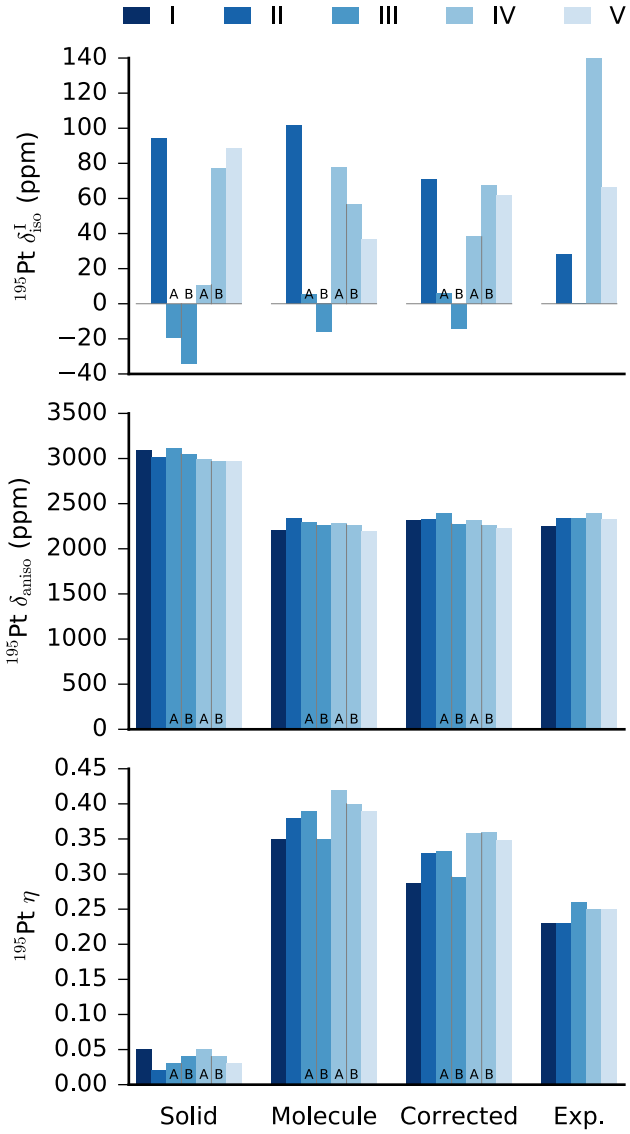

Figure 6: Comparison of the calculated and experimental values of ^{195}Pt chemical shift parameters, δ_{iso} (CS, top), δ_{aniso} (CSA parameter, middle), and η (asymmetry, bottom) in compounds I–V. The three leftmost groups of bars in each panel correspond to calculations at the SR level in solid state (PBE functional), SO ZORA level in a molecular model (PBE0 functional), and the molecular results corrected with the ligand-field contribution, correspondingly. Bars annotated with A or B refer to two different conformations of the same complex in the crystallographic unit cell.

below).

Solid-state and molecular models. Relative to the other contributions, the effect of the ligand field is most notable in the isotropic ^{195}Pt CS, as shown in Figure 5. The ligand-field modification of the CS in compound III is negligible, whereas in II it is the dominant contribution of the three. The CSA and asymmetry parameters are relatively much less affected in every complex, although the absolute contributions to δ_{aniso} of compounds I and III A are still sizable (ca. 100 ppm), justifying the ligand-field correction. Careful consideration is required when estimating this contribution, because the CASTEP calculations for a molecule in vacuum using the standard pseudopotentials yields radically different CSA (ca. 3000 ppm in CASTEP vs. 2000 ppm in ADF, see Table 33 in SI) and asymmetry parameters (0.00–0.09 vs 0.15–0.28) than a molecular calculation with ADF at the SR level using the PBE functional. A similar situation is also present in Ref. 44, where a plane wave calculation (CASTEP) yields significantly larger span for the ^{195}Pt NMR spectrum of cisplatin, as compared to a molecular calculation (ADF). The span is generally not equivalent to the CSA parameter calculated here, but for spectra where δ_{xx} is close to δ_{yy}, while δ_{zz} is far removed from both, they are somewhat similar quantities. As the authors have not specified whether spin–orbit coupling is accounted for in the molecular calculation or not, and since only pure DFT functionals have been used,[44] it is difficult to assess the reason behind the discrepancy between the experimental and calculated results.

To avoid such very large errors as found here, if the ligand-field correction is taken as the difference between a solid-state and a molecular calculation, both need to be performed within CASTEP to make use of error cancellation. The problem likely stems from the core–valence partitioning of the heavy element pseudopotential: a large core is preferred due to reduced computational cost, but may lead to an unrealistic polarization of the sub-valence region and hence a discrepancy in comparison with an all-electron calculation. The disparity is more likely visible in the anisotropic CS parameters, which do not benefit from error cancellation similarly as the isotropic chemical shift. A rigorous approach to correct the issue would be the development of an optimized pseudopotential with a smaller core, as demonstrated by Truflandier et al. for the CSA parameter of vanadium in $VOCl_3$,[48] but it is outside the scope of the present study.

Hybrid DFT functional. The inclusion of exact exchange into the DFT functional yields positive contributions to the CSA parameter, and negative ones to the CS and asymmetry parameter in all complexes, as shown in Figure 5. The largest effect is the increase of ^{195}Pt δ_{aniso} in all compounds by ca. 700 ppm (ca. 30% of the total value), which is over 1.5 times as large as the absolute value of the next largest contribution, the SO coupling. In compounds IV and V, the contribution to CS (relative to compound I) is also larger than those due to either the ligand field or the SO-coupling. The absolute contribution to η is small, up to -0.1, but the relative contribution (17–28%) is still quite large due to a small value of the parameter.

Spin–orbit correction. SO-coupling decreases (increases) the ^{195}Pt CSA (asymmetry) parameters in all compounds, acting in the opposite direction as compared to the use of hybrid functional and, in most cases, the ligand field. The effect is ca. -20% for the CSA parameter in all complexes, and 120–140% (the result being ca. 0.25 in all complexes) for the asymmetry. Hence, the incorporation of SO coupling is essential for obtaining reasonable ^{195}Pt CSA and asymmetry parameters in compounds I–V.

^{195}Pt–^{31}P spin–spin J-coupling

The spin–spin coupling constants $^2J(^{195}\mathrm{Pt}–^{31}\mathrm{P})$, calculated at the molecular SO-ZORA/PBE0 level of theory, are listed in Table 1. They are invariably determined to have the negative sign, with the absolute values in the range 401–428 Hz, close to the experimental values in the range 431–456 Hz. Relative to this, the differences between the complexes are small, down to only few Hz.

Table 3: Calculated and experimental $^2J(^{195}\mathrm{Pt}–^{31}\mathrm{P})$ spin–spin J-coupling constants in compounds I–V. Values in Hz.

Compound[a]	Calc.[b]	Exp.[c]
I	−428	444.4
II	−401	431.1±0.7
III A	−410	443.2±0.5
III B	−416	
IV A	−407	ca. 456
IV B	−403	
V	−411	433.2±0.5

[a]Pt-dtp-R, R: ethyl (I), *iso*-propyl (II), *iso*-butyl (III), *sec*-butyl (IV), and *cyclo*-hexyl (V). A and B refer to calculations on two different conformations of the same complex.
[b]ADF SO-ZORA calculation with the PBE0 hybrid functional, using optimized geometry (ions and cell parameters, CASTEP).
[c]Previously reported values. See Ref. 12 (I and IV), 10 (II and V), and 9 and 11 (III).

Geometry optimization. Geometry optimization of hydrogen had only a negligible effect of about +3 Hz (compound V) or less to the spin–spin coupling constants (see Table 35 in SI). Full optimization of ions and cell parameters caused slightly larger, but still small changes to the parameter, circa +15 Hz (compound IV A) or less.

Hybrid DFT functional. The use of a hybrid functional was found to be vital for obtaining values of J that are even remotely close to experimental observations (see the columns PBE and PBE0 in Table 35 in SI). Pure DFT (PBE) coupling constants were only of the order of −250 Hz at both SR and SO ZORA level of theory, i.e., the inclusion of 25% of exact exchange in PBE0 resulted in a 63–78% increase of the magnitude of the coupling, depending on the complex.

Relativistic effects and spin–orbit correction. The SO coupling yields negligible corrections (only few Hz) to the spin–spin coupling constants (see Table 35 in SI), as compared to the other contributions. Scalar relativistic effects are much larger, of the order of 100 Hz, compared to the NR values.

Orientation and shape of the CS tensors

In addition to the CS tensor parameters, also the principal axis directions of the tensors are obtained from calculations. A graphical example, in arbitrary scale, is represented in Figure 7 for complex V. For complexes I–V, the full shielding tensors are given in SI (see

Tables 36–42), from which the principal axes are obtained by diagonalizing the symmetric part of the tensor. In practice, the ^{195}Pt shielding tensor resembles an axial disc in the nearly planar central region of the molecule formed by the sulfur atoms, with the least-shielded component roughly perpendicular to that plane. The tensor retains its general shape and orientation in the present complexes; the least-shielded direction remains practically invariant in the molecular frame of reference, and the two most shielded components remain nearly equal in size to each other.

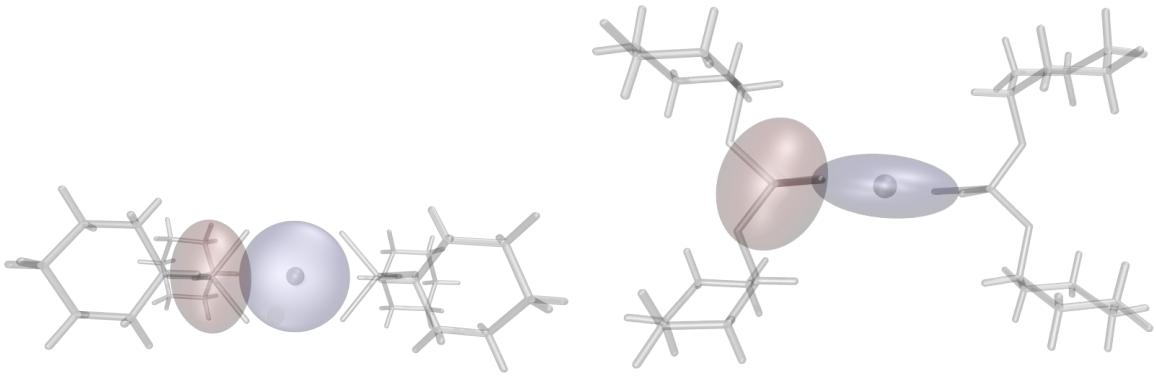

Figure 7: Illustration of the shapes of the shielding tensors of ^{195}Pt (blue, at the center of the molecule) and ^{31}P nuclei in Pt-dtp-*cyclo*-hexyl (compound V), from the top (left picture) and side (right picture) views as referenced to the SPS plane, based on a scalar-relativistic solid-state calculation with the PBE functional. The ellipsoids are drawn using the principal components of the shielding tensor of the corresponding nucleus as the three axes. The absolute sizes of the ellipsoids are not comparable between ^{195}Pt and ^{31}P, as the scale is chosen separately for each nucleus for visual purposes.

On the other hand, the ^{31}P tensor is rhombic, with the most-shielded component nearly perpendicular to the two P–O bonds in most compounds, with the two other principal components lying roughly along one of the P–O bonds, the P–Pt direction, or between these, depending on the complex and the level of calculation. A slight exception to this is the X-ray structure of compound IV (both conformations A and B), where the most-shielded direction of the phosphorus shielding tensor is considerably tilted towards the far end of a C_4H_9 ligand. However, after the geometry optimization of all ions, this tilt angle is noticeably reduced, and the tensor orientation is brought closer to that in the other compounds. By combining that with the information on the CSA parameter before and after the ion optimization, it allows one to estimate that an optimization is required to obtain agreement with experiment for the shielding tensor.

The SO and hybrid functional corrections introduce only small changes to the orientation of the ^{195}Pt and ^{31}P shielding tensors in the molecular frame of reference. The directions of the least-(most-) shielded principal components remain effectively unchanged in each complex, limiting the variation between the different levels of computation to an apparent rotation of two of the principal components around the invariant component. For ^{195}Pt, this is physically insignificant due to the disc-like shape of the shielding tensor. In the ^{31}P case, the differences are more perceptible, but still small.

Conclusions

The ^{195}Pt CSA parameter, δ_{aniso}, and the asymmetry parameter, η, of the previously obtained platinum(II) complexes with five different dialkyldithiophosphate ligands, namely, *O*,*O*′-diethyldithiophosphate, *O*,*O*′-di-*iso*-propyldithiophosphate, *O*,*O*′-di-*iso*-butyldithiophosphate, *O*,*O*′-di-*sec*-butyldithiophosphate and *O*,*O*′-di-*cyclo*-hexyldithiophosphate were determined for the first time by field-sweep NMR.

Calculations revealed that while the molecular model is a good starting point, allowing the incorporation of the spin–orbit coupled relativistic effects and exact exchange through a hybrid DFT functional, the effect of the crystal lattice is also important to the CS tensor parameters of ^{195}Pt and ^{31}P. The pseudopotential approach in solid state, however, was found to produce unreliable CS tensors for the heavy metal in complexes I–V due to the pseudopotential core being too large, resulting in an unrealistic subvalence polarization. This yielded greatly overestimated CSA and underestimated asymmetry parameters in the present systems, as verified by comparisons to molecular calculations at the same level, as well as experimental observations. The pseudopotentials available in standard software may thus be inadequate for periodic calculations of anisotropic NMR parameters. Great care is therefore needed when estimating the crystal field effect to the anisotropic CS parameters for heavy elements using a pseudopotential approach.

The platinum CSA and asymmetry parameters were found to be highly similar in all the systems, with computations certifying the experimental observation of an axial tensor shape. The directional data indicate that the smallest ^{195}Pt shielding component is nearly perpendicular to the central plane consisting of sulfur atoms in all the complexes. The computational phosphorus shielding tensors were found to be in a good agreement with experimental observations, replicating the nearly rhombic character of the tensors as well as the CSA and asymmetry parameters. Qualitative agreement was found between the calculated and experimental spin–spin *J*-coupling constants, with an unanimously negative sign of the parameter visible in all calculations.

Scalar relativistic effects were estimated using the X-ray structures, and were found to be important in all the systems, yielding (depending on the complex) absolute changes of 2–5% (14–34%) to the CSA parameter of ^{195}Pt (^{31}P), and of 7–50% (46–600%) to the asymmetry parameter, correspondingly. The inclusion of SO-coupling and the use of a hybrid functional were also found important, especially for the ^{195}Pt CS parameters. The ligand-field effect was relatively more important for the phosphorus-31 CS parameters than those of the platinum-195, but the absolute contribution was non-negligible for both nuclei. The hybrid functional was also vital for the spin–spin *J*-coupling constant, accounting for circa 63–78% of the total value of the parameter, more than the SR effects.

Based on the results, the shape and orientation of the ^{195}Pt shielding tensor is not much affected by the ligands in the studied complexes. In contrast to that, the phosphorus shielding tensor displays a subtle dependence on the ligands, allowing an unambiguous assignment of the complexes from one another and, through combining the computational and experimental data, confirming the experimentally determined structure. The results clearly display the necessity of considering several significant factors in the NMR calculations of heavy metal-containing molecular crystals, including ligand-field and relativistic effects, as well as the exact exchange component in the DFT functional. Lacking all the necessary functionality in

any single program, a tensor component-level correction method was applied to combine the different contributions, resulting in ^{195}Pt and ^{31}P shielding tensors that agree qualitatively with experimental results.

Acknowledgement

JR thanks the Finnish Cultural Foundation for funding this research, with further support received from the National Doctoral Programme in Nanoscience (NGS-NANO), the Tauno Tönning Foundation, and University of Oulu. PL was supported by the Academy of Finland projects number 125316, 218191, 255641, and 285666, and the work of JV by the directed programme in Computational Science of the Academy of Finland, project number 258565. JVH thanks the EPSRC and the University of Warwick for partial funding of the solid-state NMR infrastructure at Warwick, and acknowledges additional support for this infrastructure obtained through Birmingham Science City: Innovative Uses for Advanced Materials in the Modern World (West Midlands Centre for Advanced Materials Projects 1 and 2), with support from Advantage West Midlands (AWM) and partial funding by the European Regional Development Fund (ERDF). CSC – IT Center for Science and the Finnish Grid Initiative project provided the computational resources.

Supporting Information Available

Cartesian coordinates for X-ray and geometry-optimized stuctures, full shielding tensors, calculated shielding tensor parameters, and spin–spin coupling constants. This material is available free of charge via the Internet at `http://pubs.acs.org/`.

References

(1) Rosenberg, B.; Vancamp, L. *Nature* **1969**, *222*, 385.

(2) Rosenberg, B. *Cancer Treat. Rep.* **1979**, *63*, 1433.

(3) Harrap, K. R. *Platinum Metals Rev.* **1984**, *28*, 14.

(4) Bleiberg, H. *British J. Cancer* **1998**, *77*, 1.

(5) Burger, H.; Loos, W. J.; Eechoute, K.; Verweij, J.; Mathijssen, R. H.; Wiemer, E. A. *Drug Resistance Updates* **2011**, *14*, 22.

(6) Gianini, M.; Caseri, W. R.; Gramlich, V.; Suter, U. W. *Inorg. Chim. Acta* **2000**, *299*, 199.

(7) Tkachev, V. V.; Atovmyan, L. O. *Koord. Khim.* **1982**, *8*, 215.

(8) Kuan, F. S.; Tiekink, E. R. T. *Acta Crystallogr. Sec. E: Struct. Rep. Online* **2004**, *60*, m1619.

(9) Ivanov, A. V.; Rodina, T. A.; Ivanov, M. A.; Gerasimenko, A. V.; Antzutkin, O. N. *Dokl. Phys. Chem.* **2008**, *423*, 311.

(10) Ivanov, A. V.; Lutsenko, I. A.; Ivanov, M. A.; Gerasimenko, A. V.; Antzutkin, O. N. *Russ. J. Coord. Chem.* **2008**, *34*, 584.

(11) Rodina, T. A.; Lutsenko, I. A.; Gerasimenko, A. V.; Ivanov, A. V. *Russ. J. Coord. Chem.* **2009**, *35*, 534.

(12) Rodina, T. A.; Ivanov, A. V.; Gerasimenko, A. V.; Lutsenko, I. A.; Ivanov, M. A.; Hanna, J. V.; Antzutkin, O. N.; Sergienko, V. I. *Polyhedron* **2011**, *30*, 2210.

(13) Ivanov, A. V.; Palazhchenko, V. I.; Strikha, V. E.; Antzutkin, O. N.; Forsling, W. *Dokl. Earth. Sci.* **2006**, *410*, 1141.

(14) Rozhdestvina, V. I.; Ivanov, A. V.; Zaremba, M. A.; Antzutkin, O. N.; Forsling, W. *Crystallogr. Reports* **2008**, *53*, 391.

(15) Rees, G. J.; Orr, S. T.; Barrett, L. O.; Fisher, J. M.; Houghton, J.; Spikes, G. H.; Theobald, B. R.; Thompsett, D.; Smith, M. E.; Hanna, J. V. *Phys. Chem. Chem. Phys.* **2013**, *15*, 17195.

(16) Sindorf, D. W.; Bartuska, V. J. *J. Magn. Reson.* **1989**, *85*, 581.

(17) Fu, L.-j.; Vaara, J. *ChemPhysChem* **2014**, *15*, 2337.

(18) Fedorov, S. V.; Rusakov, Y. Y.; Krivdin, L. B. *Magn. Reson. Chem.* **2014**, *52*, 699.

(19) Orr, S. T. *Multinuclear solid-state NMR of fuel cell materials*; Warwick University, 2010.

(20) Massiot, D.; Fayon, F.; Capron, M.; King, I.; Le Calvé, S.; Alonso, B.; Durand, J.-O.; Bujoli, B.; Gan, Z.; Hoatson, G. *Magn. Reson. Chem.* **2002**, *40*, 70.

(21) Turner, G. L.; Smith, K. A.; Kirkpatrick, R. J.; Oldfieldt, E. *J. Magn. Reson.* **1986**, *70*, 408.

(22) Antzutkin, O. N.; Lee, Y.; Levitt, M. *J. Magn. Reson.* **1998**, *135*, 144.

(23) Wolfram, S. *The Mathematica Book*; Cambridge University Press, 1999.

(24) Clark, S. J.; Segall, M. D.; Pickard, C. J.; Hasnip, P. J.; Probert, M. J.; Refson, K.; Payne, M. C. *Zeitschrift für Kristallographie* **2005**, *220*, 567.

(25) Pickard, C. J.; Mauri, F. *Phys. Rev. B* **2001**, *63*, 245101.

(26) Yates, J. R.; Pickard, C. J.; Payne, M. C.; Mauri, F. *J. Chem. Phys.* **2003**, *118*, 5746.

(27) Yates, J. R.; Pickard, C. J.; Mauri, F. *Phys. Rev. B* **2007**, *76*, 024401.

(28) (a) Schreckenbach, G.; Ziegler, T. *J. Phys. Chem.* **1995**, *99*, 606; (b) ADF2013, SCM, Theoretical Chemistry, Vrije Universiteit, Amsterdam, The Netherlands.; (c) ADF2014, SCM, Theoretical Chemistry, Vrije Universiteit, Amsterdam, The Netherlands, `http://www.scm.com`.

(29) Krykunov, M.; Ziegler, T.; van Lenthe, E. *Int. J. Quantum Chem.* **2009**, *109*, 1676.

(30) Wolff, S. K.; Ziegler, T. *J. Chem. Phys.* **1998**, *109*, 895.

(31) Wolff, S. K.; Ziegler, T.; van Lenthe, E.; Baerends, E. J. *J. Chem. Phys.* **1999**, *110*, 7689.

(32) (a) van Lenthe, E.; Baerends, E. J.; Snijders, J. G. *J. Chem. Phys.* **1993**, *99*, 4597; (b) van Lenthe, E.; Baerends, E. J.; Snijders, J. G. *J. Chem. Phys.* **1994**, *101*, 9783.

(33) Bonhomme, C.; Gervais, C.; Babonneau, F.; Coelho, C.; Pourpoint, F.; Azaïs, T.; Ashbrook, S. E.; Griffin, J. M.; Yates, J. R.; Mauri, F.; Pickard, C. J. *Chem. Rev.* **2012**, *112*, 5733.

(34) (a) ReSpect, version 3.4.1 (beta), 2014; Relativistic Spectroscopy DFT program of authors Repisky, M.; Komorovsky, S.; Malkin, V. G.; Malkina, O. L.; Kaupp, M.; Ruud K., with contributions from Bast, R.; Ekström, U.; Knecht S.; Malkin Ondik, I.; Malkin, E. (see `http://rel-qchem.sav.sk`); (b) Komorovsky, S.; Repisky, M.; Malkina, O. L.; Malkin, V. G.; Malkin Ondík, I.; Kaupp, M. *J. Chem. Phys.* **2008**, *128*, 104101; (c) Komorovsky, S.; Repisky, M.; Malkina, O. L.; Malkin, V. G. *J. Chem. Phys.* **2010**, *132*, 154101.

(35) van Lenthe, E.; Baerends, E. J. *J. Comput. Chem.* **2003**, *24*, 1142.

(36) (a) Dyall, K. G. *Theor. Chem. Acc.* **2004**, *112*, 403; (b) Dyall, K. G.; Gomes, A. S. P. *Theor. Chem. Acc.* **2010**, *125*, 97; (c) Dyall, K. G. *Theor. Chem. Acc.* **2012**, *131*, 1217; (d) K. G. Dyall, unpublished. Basis sets are available from the Dirac web site, `http://dirac.chem.sdu.dk`.

(37) Perdew, J. P.; Burke, K.; Ernzerhof, M. *Phys. Rev. Lett.* **1996**, *77*, 3865, Erratum Ibid. **1997**, *78*, 1396.

(38) Ernzerhof, M.; Scuseria, G. E. *J. Chem. Phys.* **1999**, *110*, 5029.

(39) Adamo, C.; Barone, V. *J. Chem. Phys.* **1999**, *110*, 6158.

(40) Vanderbilt, D. *Phys. Rev. B* **1990**, *41*, 7892.

(41) Straka, M.; Lantto, P.; Vaara, J. *J. Phys. Chem. A* **2008**, *112*, 2658.

(42) Roukala, J.; Maldonado, A. F.; Vaara, J.; Aucar, G. A.; Lantto, P. *Phys. Chem. Chem. Phys.* **2011**, *13*, 21016.

(43) Mastrorilli, P.; Todisco, S.; Bagno, A.; Gallo, V.; Latronico, M.; Fortuño, C.; Gudat, D. *Inorg. Chem.* **2015**, *54*, 5855.

(44) Lucier, B. E. G.; Reidel, A. R.; Schurko, R. W. *Can. J. Chem.* **2011**, *89*, 919.

(45) Pecul, M.; Urbańczyk, M.; Wodyński, A.; Jaszuński, M. *Magn. Reson. Chem.* **2011**, *49*, 399.

(46) Pyykkö, P.; Görling, A.; Rösch, N. *Mol. Phys.* **1987**, *61*, 195.

(47) Kaupp, M.; Malkina, O. L.; Malkin, V. G.; Pyykkö, P. *Chem. Eur. J.* **1998**, *4*, 118.

(48) Truflandier, L.; Paris, M.; Boucher, F. *Phys. Rev. B* **2007**, *76*, 035102.

Graphical TOC Entry

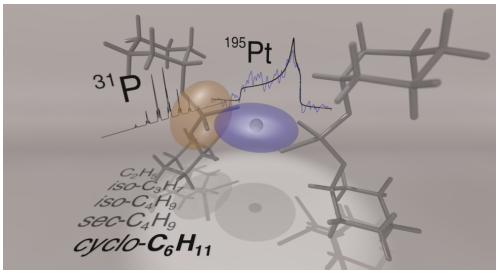

Polycrystalline bis(dialkyldithiophosphato)Pt(II) complexes with five different O,O'-dialkyldithiophosphate ligands were studied using solid-state ^{31}P and ^{195}Pt NMR, as well as theoretical calculations at hybrid DFT level including spin–orbit relativistic and crystal lattice effects, to reveal the influence of the ligand substituents to the central PtS_4 chromophore structure, as well as the shapes and orientations of the ^{31}P and ^{195}Pt chemical shift tensors.